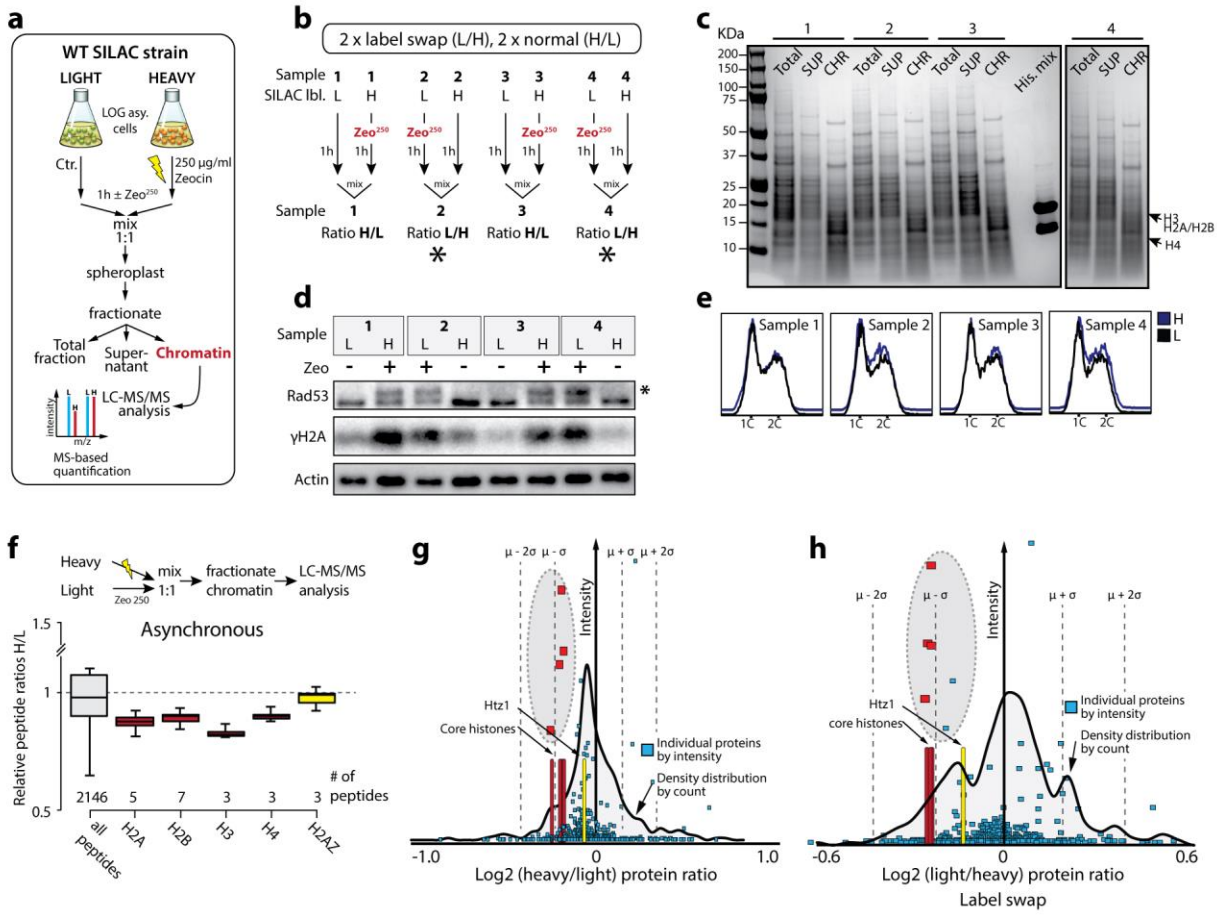

Supplementary Figure 1

SILAC mass spectrometry of pre-enriched chromatin depicts core histone loss.

(**a**) Experimental workflow for SILAC mass spectrometry after Zeocin treatment. (**b**) Labeling and mixing of samples from 4 individual experiments. Asterisks indicates label swap (**c**) Colloidal Commassie stained SDS-PAGE of SILAC experiment replicas showing total protein, supernatant (SUP), and chromatin (CHR) fractions from **a**. His. mix is an equimolar mixture of recombinant Histone H2A, H2B, H3 and H4. (**d**) Control Immunoblot analysis using anti-γH2A anti-Rad53 antibodies to show that checkpoint is activated after Zeocin treatment in the SILAC samples from **bc. (e**) FACS analysis showing that all samples from **b-d** have similar cell cycle profiles. Actin was used as loading control. Asterisks indicate the phosphorylation-dependent mobility shift of Rad53. (**f**) SILAC mass spectrometry on chromatin fractions from three independent cell pools. Boxplots show heavy/light histone peptide distribution indicating the degradation of core histones and, to a lesser extent, Htz1 (H2A.Z). (**g**) Distribution of measured protein ratios in the non-label swap experiment or (**h**) label swap experiment. Core histones are labelled red and reside within the µ-σ range. Htz1 is labelled yellow and resides closer to the mean ratio of all proteins. Boxplots in **f** represent median values, interquartile ranges and whiskers.

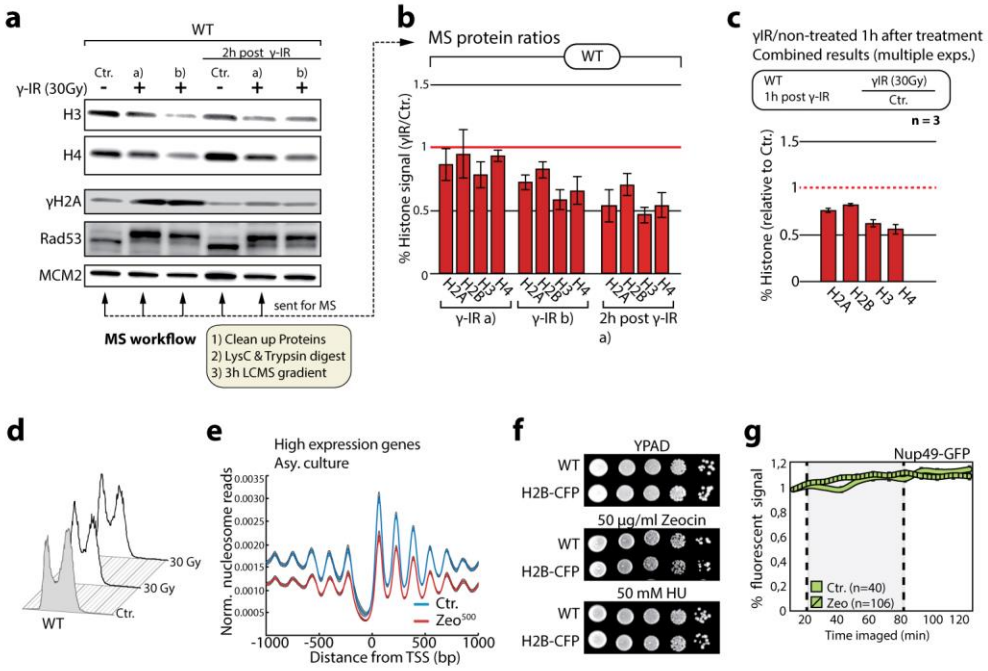

Supplementary Figure 2

Gamma irradiation triggers degradation of core histones, Zeocin reduces nucleosome occupancy, and H2B-CFP tagging does not interfere with cell viability.

(**a**) Immunoblot analysis from one experiment using H3 and H4 specific antibodies on whole cell extracts of asynchronous WT cells exposed to 30 Gy gamma irradiation (γ-IR). Rad53 and γH2A were probed to confirm checkpoint activation. MCM2 was used to control for loading. Arrows indicate samples sent for label-free quantitative mass spectrometric analysis. (**b)** Label-free quantitative mass spectrometry results of samples depicted in **a**. Bar graphs show mean peptide ratios ± s.e.m for the indicated histone proteins upon γIR exposure relative to the control condition. (**c**) Combined label-free mass spectrometry results of sample γ-IR a), γIR b) and an additional experiment. Bar graphs represent the mean peptide ratios (γIR/Ctr.) ± s.e.m. for core histones over all samples. (**d**) FACS analysis showing that all samples have similar cell cycle profiles. (**e**) Genome-wide nucleosome mapping graph shows the distribution of nucleosome reads over 750 highly expressed genes aligned to their TSS from four independent experiments (±s.d. is shaded). (**f**) Drop assay control showing that the H2B-CFP fusion complements the absence of H2B in response to genotoxic agents. (**g**) Live single-cell microscopy of Nup49-GFP. Graph shows the the mean fluorescent signals of of all individual cells (cell numbers indicated in graph) per treatment over time relative to the control (Ctr.) condition. Dotted lines indicate the duration of Zeocin treatment. Graphs show mean ± s.e.m..

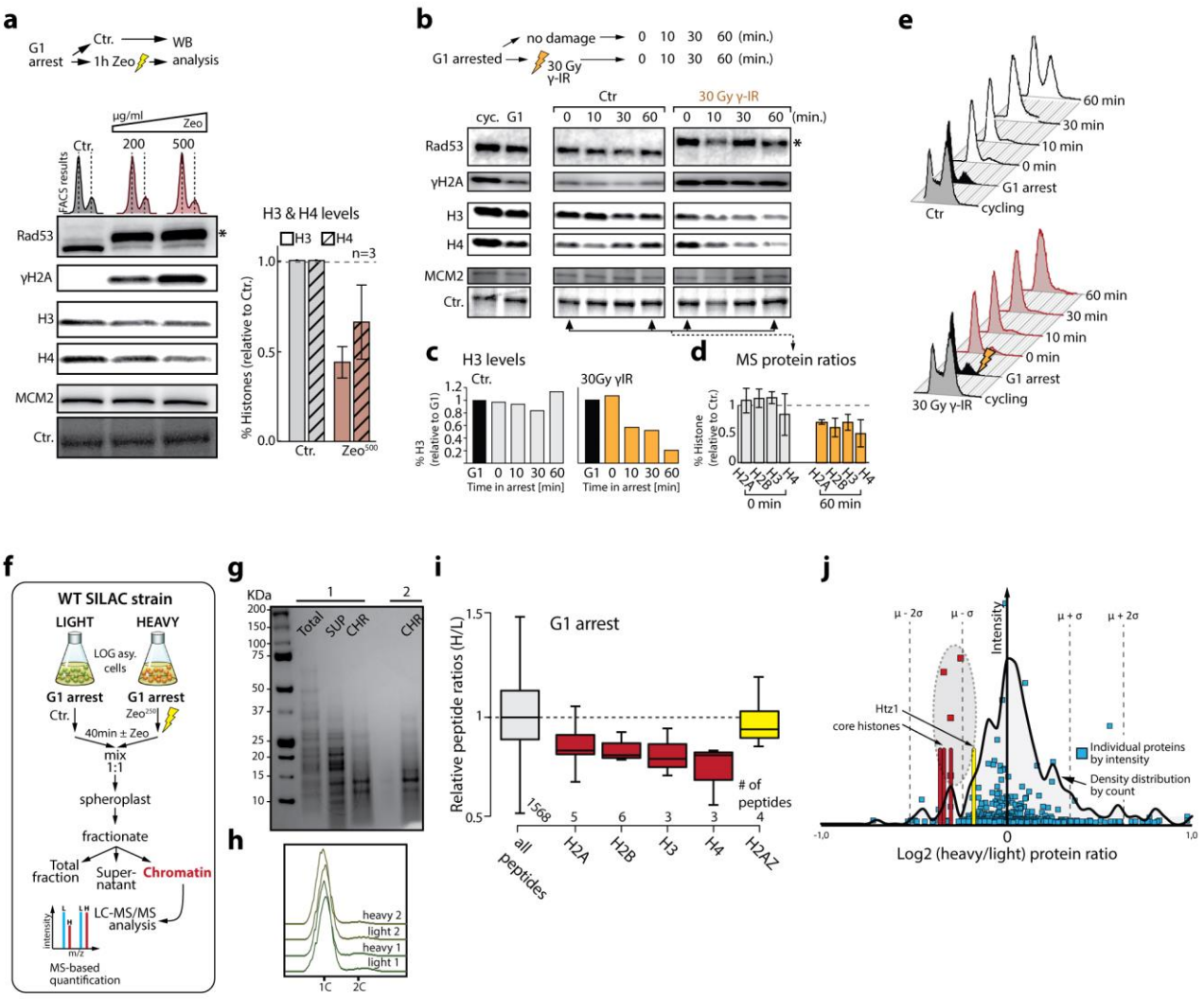

Supplementary Figure 3

Damage-induced histone loss occurs in G1 phase.

(**a-b**) Representative immunoblot analysis of whole cell extracts from G1-arrested cells treated with Zeocin **a** or after exposure to γIR **b**. Histone H3 and H4 levels were probed using histone specific antibodies. Rad53 and γH2A were probed to confirm checkpoint activation. MCM2 was used to control for loading and Ctr. represents bands on the ponceau stained membrane. Bar graphs in **a** show the mean ± s.e.m. over three independent replicates relative to the control condition. FACS results of Zeocin treated samples are shown above immunoblots in **a**. Arrows in **b** indicate samples sent for label-free quantitative mass spectrometric analysis. (**c**) Immunoblot quantifications of irradiated samples from one experiment marked with arrows. (**d**) Label-free quantitative mass spectrometry results of samples depicted with arrows. Bar graphs show mean peptide ratios ± s.e.m. for the indicated histone proteins upon γIR exposure relative to the control condition. (**e**) FACS analysis showing cell cycle profiles of all samples from **b**. (**f**) Experimental workflow for SILAC mass spectrometry of G1 arrested cells after Zeocin treatment. (**g**) Commassie stained SDS-PAGE of samples showing total protein, supernatant (SUP), and chromatin (CHR) fractions. (**h**) FACS analysis showing similar G1 arrest efficiency for all samples. (**i**) SILAC mass spectrometry on chromatin fractions from two independent cells pools. Boxplots show heavy/light histone peptide distribution indicating the degradation of core histones and, to a lesser extent, Htz1. (**j**) Distribution of measured proteins ratios. Core histones are labelled red and reside within the µ-σ range. Htz1 is labelled yellow and residues closer to the mean ratio of all proteins. Boxplots in **i** represent median values, interquartile ranges and whiskers. Asterisk indicates phosphorylation-dependent Rad53 mobility shift.

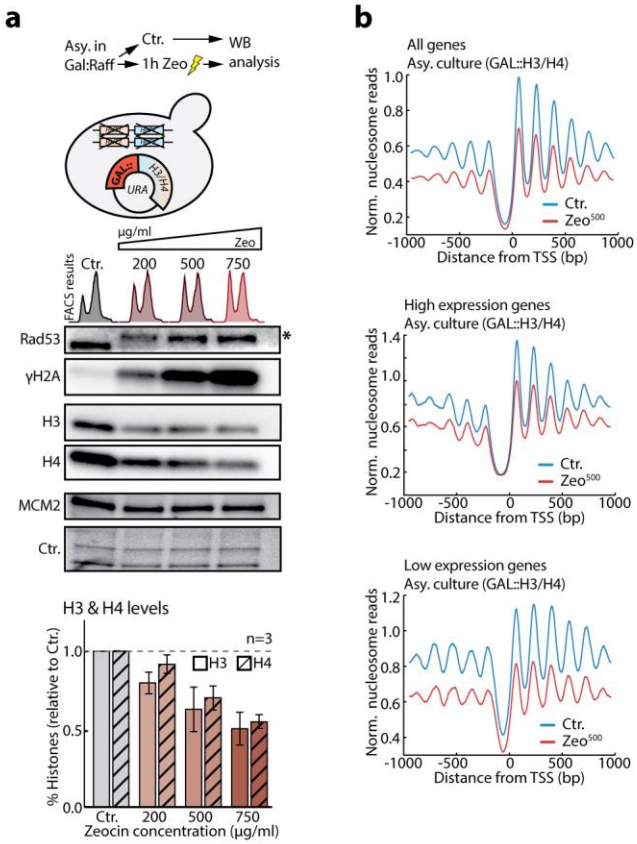

Supplementary Figure 4

Damage-induced histone loss is independent of histone transcription.

(**a**) Top panel shows the experimental procedure and strain used for constitutive histone H3 and H4 transcription in cells grown in YPGal:Raff medium (strain GA-8386). A *URA3* plasmid borne construct in which the *GAL1-10* promoter drives the only pair of histone H3/H4 genes is used. Mid panel shows representative immunoblot analysis using anti-H3 and anti-H4 antibodies on whole cell extracts from the strain depicted in **a** after Zeocin treatment and growth in YPGal:Raff medium. Rad53 and γH2A were probed to confirm checkpoint activation. MCM2 was used to control for loading and Ctr. represents bands on the original gel (UV-TGX stained). Bar graphs in bottom panel show the mean ± s.e.m. over three independent replicates relative to the control condition. Asterisk indicates phosphorylation-dependent Rad53 mobility shift. (**b**) Zeocin treatment causes a genome-wide decrease in nucleosome occupancies. Data represents nucleosome occupancies over the total pool of 5014 protein coding genes, 750 high expression genes and 750 low expression genes aligned to their transcriptional start site (TSS) from one experiment using the strain depicted in **a**.

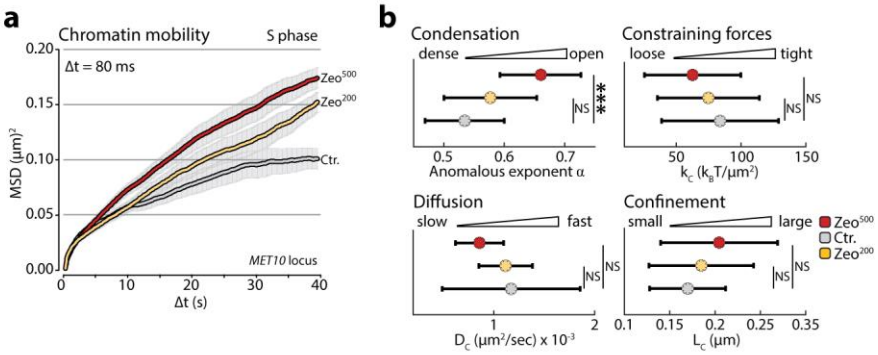

Supplementary Figure 5

High-speed, live-cell imaging reveals increased chromatin movement and a loss of constraining forces after DNA damage.

(**a**) High-speed (Δt=80 ms) imaging of the undamaged *MET10* locus (as in **Fig. 3a-b**) showing that chromatin mobility increases with Zeocin concentration. Average MSD graphs indicate dose-dependent increases in global chromatin mobility in response to DNA damage ($n^{Ctr.}$=39, n^{Zeo200}=31, n^{Zeo500}=29 different cells from three independent experiments). (**b)** Graphs show the means and whiskers (±s.d.) of biophysical parameters derived from imaging data and predict chromatin decompaction after Zeocin treatment. P-values, ***P<0.001, NS=not significant, result from Kolmogorov-Smirnov-tests. All MSD graphs represent the mean ± s.e.m. of cells pooled from three independent experiments. Additionally, consult Supplementary Dataset 2 for mobility parameters and the number of cells analyzed.

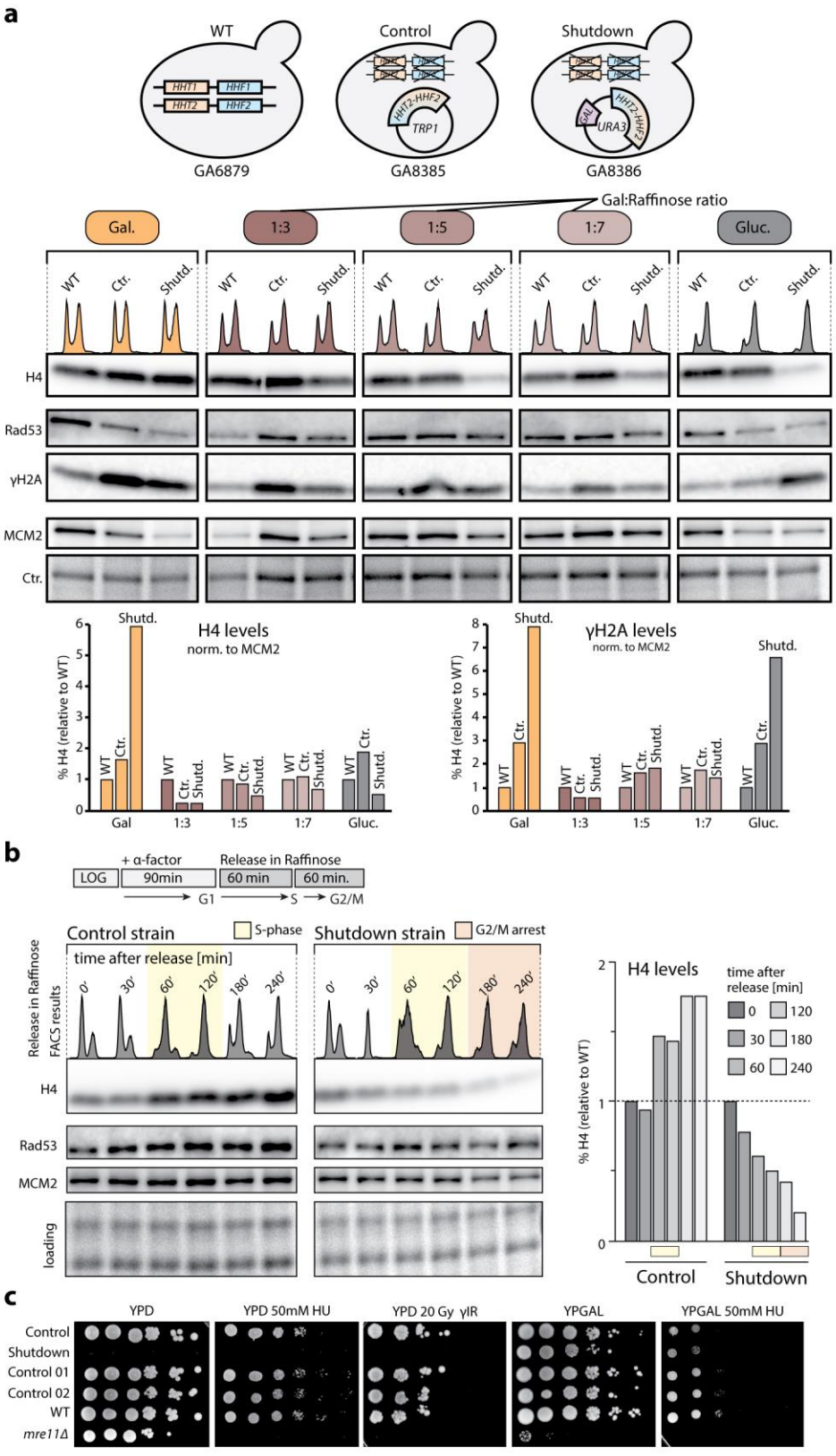

Supplementary Figure 6

GAL::H3/H4 strain as a tool for *in vivo* artificially controlled histone-level reductions.

(**a**) Schematic representation of wild-type, control and shutdown strains grown in the indicated media. Gal. = galactose, gluc. = glucose. Immunoblot analysis of whole cell extracts of the indicated conditions and strains were performed using an antibody directed against Histone H4. Rad53 and γH2A were probed to confirm checkpoint activation. MCM2 was used to control for loading. Bar graphs from quantified immunoblot derived from one experiment shows overexpression or reduction of H3/H4 in the shutdown strain grown in gal. or gluc. medium respectively. Growth of the shutdown strain in Gal:Raff 1:5 confers H3/H4 levels similar to WT. (**b**) Experimental workflow of the arrest-release experiment used to reduce histone levels in S phase (as in **Fig. 5**). Bar graphs from quantified immunoblot data derived from one experiment shows reductions of H3 and H4 upon release into raffinose medium. (**c**) A defined number of exponentially growing cells (fivefold dilutions) was spotted on different YP or YPD plates containing the indicated dose of hydroxyurea (HU). Cells exposed to 20 Gy γIR were spotted onto YPD plates. Drop assays show functionality of shutdown and control strains. Control = control from **a**, control 1 and 2 = similar to control 1 but expressing HHT2-HHF2 from a *URA3* plasmid (**a**).

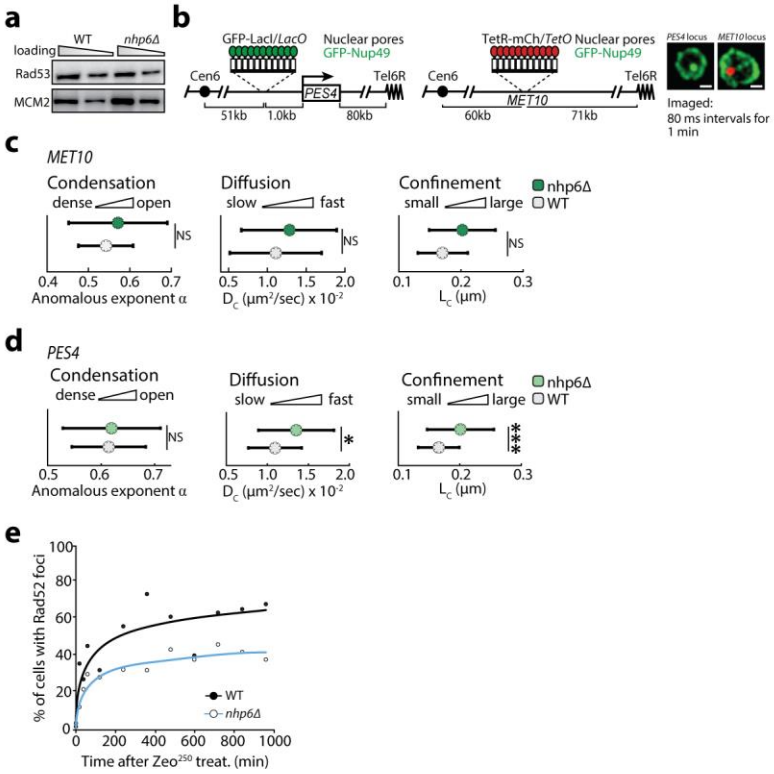

Supplementary Figure 7

Biophysical parameters of *nhp6*Δ tracking data and results from Rad52-YFP recovery assay.

(**a**) Control Immunoblot from one experiment (loading 1x and 2x the volume) showing that *nhp6Δ* strains do not have constitutive checkpoint activation. Rad53 was probed to test for checkpoint activation and MCM2 was used as loading control. (**b**) Schematics of the strains used for imaging the *PES4* and *MET10* loci (**Fig. 6c-e**) with representative images. Scale bar is 2 μm. (**c-d**) Graphs show the means and whiskers (±s.d.) of biophysical parameters derived from imaging data of *PES4* **c** and *MET10* **d** (**Fig. 6c,d**). P-values, *P<0.05, ***P<0.001, NS=not significant, result from Kolmogorov-Smirnov-Tests. (**e**) Rad52-YFP foci recovery assay. Graph shows the overall percentage of Rad52-YFP foci containing cells for each of the 12 time-points from one experiment plotted against the time and shown together with a logarithmic fit.

Supplementary Tables

Nucleosome mapping sequencing reads

Supplementary Table 1: Information on sequencing reads obtained for each nucleosome mapping replicate. The strain column indicates the strains used. GA-6879 is the wild type and GA-8386 the shutdown strain grown in galactose:raffinose medium. A-C in the strain column indicates the four independent experiments with or without Zeocin treatment for 1h prior to MNase digestion. Column A shows the *S. Cerevisiae* reads and column B the reads from the *C. glabrata* spike-in control.

	A	B	C=(A+B)	E=(A/C)	F=(B/C)*100
Strain	***S. ce.***	***C. glab.***	**total**	**Read fraction *S. cer.***	**Read fraction *C. glab.***
GA-6879_A	50692473.00	9866228.00	60558701.00	0.84	0.16
GA-6879_A_Zeocin	46090144.00	13483686.00	59573830.00	0.77	0.23
GA-6879_B	38787017.00	7282715.00	46069732.00	0.84	0.16
GA-6879_B_Zeocin	36619974.00	10714730.00	47334704.00	0.77	0.23
GA-6879_C	34427922.00	6626795.00	41054717.00	0.84	0.16
GA-6879_C_Zeocin	29746798.00	7722737.00	37469535.00	0.79	0.21
GA-6879_D	25931187.00	4679458.00	30610645.00	0.85	0.15
GA-6879_D_Zeocin	43185379.00	12185328.00	55370707.00	0.78	0.22
GA-8386_A	82089867.00	21788485.00	103878352.00	0.79	0.21
GA-8386_A_Zeocin	53677477.00	20342128.00	74019605.00	0.73	0.27
GA-8386_B	41546073.00	9859227.00	51405300.00	0.81	0.19
GA-8386_B_Zeocin	32786223.00	12332953.00	45119176.00	0.73	0.27
GA-8386_C	25328106.00	6741373.00	32069479.00	0.79	0.21
GA-8386_C_Zeocin	27560758.00	10640545.00	38201303.00	0.72	0.28
GA-8386_D	30336089.00	7284044.00	37620133.00	0.81	0.19
GA-8386_D_Zeocin	31958581.00	12219914.00	44178495.00	0.72	0.28

Nature Structural & Molecular Biology: doi:10.1038/nsmb.3347

Yeast strains used in this study

Supplementary Table 2: Yeast strains used in this study. All strains are haploid and all except the SILAC strain and the Htz1-mEos imaging control are derived from the W303 background.

Strain number	Genotype	Source
BY	*MAT**a***; *his3del200*; *leu2del0*; *met15del0*; *trp1del63*; *ura3del0*; (BY4733)	exemplary genotype
W303	*MAT**a***; *ade2-1*; *trp1-1*; *his3-11*; *his3-15*; *ura3-1*; *leu2-3*; *leu2-112*; (W303)	exemplary genotype
JKM179	*MAT**α***; *hml::ADE1*; *hmr::ADE1*; *ade3::GALHO*; *leu2-3*; *lys5 trp1::hisG*; *ura3-52* (JKM179)	exemplary genotype
yAG-06A	*YHR018c::kanMX4*; *YIR034c::kanMX4* (BY4733)	[1]
GA-6879	*MAT**a**, RAD52-YFP*; *NUP49-GFP*; *ADE2::TetR-mCherry*; *lys5::LacI-CFP::TRP*; *leu2::LoxP*; *ZWF1:cutsite(Lmn::lys5::IsceIcs::LEU2::LacO array::Lmn)*; *met10::lmn adaptamers::HIS3::TetOps-LexA* (W303)	[2]
GA-9773	*MAT**a***; *PES4::4xLexA-lacO::TRP1*; *his3-15::GFP-LacI-HIS3*; *NUP49-GFP*	This study
GA-9774	*nhp6a::kanMX4*; *nhp6b::kanMX4*, same as GA-9773	This study
GA-9771	*nhp6a::kanMX4*; *nhp6b::kanMX4*, same as GA-6879	This study
GA-9815	*arp8::NAT,* same as GA9771	
GA-9772	Isogenic to GA-6879	This study
GA-7553	*sml1::HIS3*; same as GA-6879	This study
GA-8132	arp8::NAT; same as GA-6879	This study
GA-8182	ies4::NAT; same as GA-6879	This study
GA-8185	swr1::NAT; same as GA-6879	This study
GA-8202	arp5::NAT; same as GA-6879	This study
GA-7551	*rad51::NAT*; in GA-6879	This study
GA-7552	*rad53::NAT*; same as GA-7553	This study
GA-7556	*mec1::NAT*; same as GA-7553	This study
GA-8385	*MAT**a***; *Nup49-GFP*; *GFP-LacI::HIS3*; *hht2-hhf2Δ hht1-hhf1Δ(no marker) + [#3495 pDM18 pRS415*; *HHT2-HHF2*; *CEN/ARS, TRP1]* (W303)	This study
GA-8386	*MAT**a***; *Nup49-GFP*; *GFP-LacI::HIS3*; *hht2-hhf2Δ hht1-hhf1Δ(no marker) + [#3484 pRM102 pUK420*; *GAL10-HHT2 GAL1-HHF2*; *CEN/ARS, URA3]* (W303)	This study
GA-8387	*MAT**a***; *Nup49-GFP*; *GFP-LacI::HIS3*; *hht2-hhf2Δ hht1-hhf1Δ(no marker) + [#3494 pDM9 pRS416*; *HHT1-HHF1*; *CEN/ARS*; *URA3]* (W303)	This study
GA-9775	*LacO::LEU2::MGS1*, same as GA8385	This study
GA-9776	*LacO::LEU2::MGS1*, same as GA8386	This study
GA-3364	*MAT**a***; *HTB2-CFP::kanXM* (W303)	Brian Luke
GA-9700	*rad51::URA3*; same as GA-3364	This study
GA-9698	*sml1::URA3*; same as GA-3364	This study
GA-9695	*arp8::natMX*; same as GA-3364	This study
GA-9712	*Rad53::natMX*; same as GA-9712	This study
GA-9594	*MAT**α***; *Htz1-Eos::URA3*; same as JKM179	This study
GA-5816	*MAT**α***; *Rad52-YFP*; *NUP49-GFP*; *HIS3::LacI-GFP* (W303)	This study
YMB08 (GA-9227)	*MAT**α***; *ura3-1::LacI-GFP-URA3*; *515kb-XIV::lacO-TRP1*; *YGL117::tetR-mRFP-NATMX*; *196kb-XIV::tetO-LEU2* (W303)	Kerstin Bystricky
GA-9777	*MAT**α***; *YGL117(ARS714)::TetR-mRFP-NAT*; *ade2-1::His3p-CFP-lacI-URA3p-LambdacI-YFP-ADE2*; *leu2-3,112 :: tetO-LEU2*; *74kb :: LambdaO-HIS3*; *40kb :: LacO-TRP1*; *RAD52-EGFP-CaURA3*	This study
GA-1365	*MAT**a**, pre1-1, pre2-2*	[3]
GA-1366	*Mat**a**,* WT strain isogenic to GA-1365 and GA-1366	[3]
GA-1364	*Mat**a**, erg6::LEU2*	[4]

Nature Structural & Molecular Biology: doi:10.1038/nsmb.3347

Plasmids used in this study

Supplementary Table 3: Plasmids used in this study

Plasmid number	Description	Type	Yeast selection	Bacterial selection	Source
#3484	pUK420-GAL10-HHT2 GAL1-HHF2	CEN/ARS	URA3	AMP	Addgene [5]
#3494	pRS416-HHT1-HHF1	CEN/ARS	URA3	AMP	[6]
#3495	pRS414-HHT2-HHF2	CEN/ARS	TRP1	AMP	[7]
#279	pRS406	integrating	URA3	AMP	Addgene
#1049	pAG32	see source	see source	see source	[8]
#1050	pAG60	see source	see source	see source	[8]
#2422	pWJ132-hphMX4-Gal1-10	2µ plasmid	ADE2/hphMX4	AMP	This study

Antibodies used in this study

Supplementary Table 4: Antibodies used in this study

Antibody	Supplier	Conditions used
Mouse α Rad53	Custom made antibody (GenScript)	1:200 in milk
Rabbit α H4	Abcam AB 10158	1:5000 or 1:7500 in BSA
Mouse α actin	MAB1501	1:10,000 in milk
Goat α MCM2	Santa Cruz (SC 6680)	1:3000 in BSA
Rabbit α γH2A	Custom made antibody	1:3000 i BSA
Rabbit α H3	Abcam AB1791	1:10,000 in BSA
Rabbit α Ubiquitin	Abcam (AB19247)	1:2000 in milk

Nature Structural & Molecular Biology: doi:10.1038/nsmb.3347

Supplementary Table References

1. Gruhler, A. et al. Quantitative phosphoproteomics applied to the yeast pheromone signaling pathway. *Mol Cell Proteomics* **4**, 310-27 (2005).
2. Seeber, A., Dion, V. & Gasser, S.M. Checkpoint kinases and the INO80 nucleosome remodeling complex enhance global chromatin mobility in response to DNA damage. *Genes Dev* **27**, 1999-2008 (2013).
3. Richterruoff, B., Wolf, D.H. & Hochstrasser, M. Degradation of the Yeast Mat-Alpha-2 Transcriptional Regulator Is Mediated by the Proteasome. *Febs Letters* **354**, 50-52 (1994).
4. Heese-Peck, A. et al. Multiple functions of sterols in yeast endocytosis. *Mol Biol Cell* **13**, 2664-80 (2002).
5. Mann, R.K. & Grunstein, M. Histone H3 N-terminal mutations allow hyperactivation of the yeast GAL1 gene in vivo. *EMBO J* **11**, 3297-306 (1992).
6. Duina, A.A. & Winston, F. Analysis of a mutant histone H3 that perturbs the association of Swi/Snf with chromatin. *Molecular and Cellular Biology* **24**, 561-572 (2004).
7. Park, J.H., Cosgrove, M.S., Youngman, E., Wolberger, C. & Boeke, J.D. A core nucleosome surface crucial for transcriptional silencing. *Nature Genetics* **32**, 273-279 (2002).
8. Goldstein, A.L. & McCusker, J.H. Three new dominant drug resistance cassettes for gene disruption in Saccharomyces cerevisiae. *Yeast* **15**, 1541-1553 (1999).

Nature Structural & Molecular Biology: doi:10.1038/nsmb.3347

Supplementary Notes

Estimating the anomalous diffusion exponent α and the diffusion coefficient

We computed the cross-correlation (CC) function using [1]:

$$C(t) = \frac{1}{N_p - t} \sum_{k=1}^{N_p - t} (\mathbf{R}_c(k\Delta t) - \mathbf{R}_c((k+t)\Delta t)^2, \tag{6}$$

for $t = 1, T-1$, where N_p is the number of points in the trajectory. In many studies the CC is referred to as the MSD function [2,3] although these two functions are distinct[1]. The MSD is defined as the squared displacement with respect to the initial trajectory position, averaged over time:

$$\text{MSD(t)} = \left\langle \left(R_c(t) - R_c(0) \right)^2 \right\rangle.$$

For short times, $C(t)$ increases as a power law

$$C(t) = Ct^{\alpha}. \tag{7}$$

where $C > 0$. To extract the coefficient α, we computed $C(t)$ from empirical trajectories and fitted the first seven points of the curve to a power law. A chromatin or DNA locus is characterized experimentally by $\alpha < 1$ [4,5], while for normal diffusion $\alpha = 1$. In the Rouse polymer model[6], the anomalous exponent is $\alpha = 0.5$ computed for intermediate time regime (see [6]).

To compute the diffusion coefficient of the tagged monomer, we use the following empirical estimator described in [1]:

$$D_c = \frac{1}{4\Delta t} \sum_{k=1}^{N_p - 1} (\mathbf{R}_c(k\Delta t) - \mathbf{R}_c((k+1)\Delta t))^2, \tag{8}$$

For short time interval $\Delta t = b^2/D$, the locus motion is Brownian and the diffusion coefficient is well approximated by eq.(8).

Nature Structural & Molecular Biology: doi:10.1038/nsmb.3347

Estimating the effective spring coefficient k_c

Because the chromatin interacts locally with its environment, we estimated this interaction using a polymer model[7], by a harmonic well of strength k acting on a single monomer $\mathbf{R}_n$. The potential energy of the interaction is

$$U(\mathbf{R}_n) = \frac{1}{2}k(\mathbf{R}_n - \boldsymbol{\mu})^2, \tag{9}$$

where $\boldsymbol{\mu}$ is the fix position of the interaction. The velocity of an observed monomer c, averaged over many trajectories is driven by this interacting force, following the relation described in [7]:

$$\lim_{\Delta t \to 0} E\{\frac{\mathbf{R}_c(t+\Delta t) - \mathbf{R}_c(t)}{\Delta t} \mid \mathbf{R}_c(t) = \mathbf{x}\} = -Dk_{cn}(\mathbf{x} - \boldsymbol{\mu}), \tag{10}$$

where $\mathbf{R}_c(t)$ is the position of locus c at time t and D the diffusion coefficient and $E\{. \mid \mathbf{R}_c(t) = \mathbf{x}\}$ means averaging over trajectory realizations such that the condition $\mathbf{R}_c(t) = \mathbf{x}$ is satisfied. Relation (18) links the average velocity of the observed monomer c to the force applied at a distance $|c - n|$. For a Rouse polymer, with a potential well of type (17), the effective spring coefficient is given by

$$k_{cn} = \frac{k\kappa}{\kappa + |c - n|k}, \tag{11}$$

where κ is the monomer-monomer spring coefficient. We estimated k_c from the empirical locus trajectories $\mathbf{R}_c(t)$ by

$$k_c \approx \frac{1}{2(N_p - 1)} \sum_{i=1}^{2} \sum_{h=1}^{N_p - 1} \frac{R_c^i((h+1)\Delta t) - R_c^i(h\Delta t)}{D_c \Delta t (R_c^i(h\Delta t) - \langle R_c^i \rangle)}, \tag{12}$$

where i is the spatial direction (in two dimensions, we sum over the x and y components) and N_p is the number of points in the trajectory. In practice, the quantity $\langle R_c^i \rangle$ is computed by averaging over the trajectory. The diffusion coefficient D_c can be computed by using eq. 8.

Nature Structural & Molecular Biology: doi:10.1038/nsmb.3347

Supplementary Notes References

1. Schuss, Z. Diffusion and Stochastic Processes. An Analytical Approach. *Springer-Verlag, New York, NY* (2009).
2. Dion, V., Kalck, V., Horigome, C., Towbin, B.D. & Gasser, S.M. Increased mobility of double-strand breaks requires Mec1, Rad9 and the homologous recombination machinery. *Nat Cell Biol* **14**, 502-9 (2012).
3. Mine-Hattab, J. & Rothstein, R. Increased chromosome mobility facilitates homology search during recombination. *Nat Cell Biol* **14**, 510-7 (2012).
4. Kepten, E., Bronshtein, I. & Garini, Y. Improved estimation of anomalous diffusion exponents in single-particle tracking experiments. *Physical Review E* **87**(2013).
5. Weber, S.C., Theriot, J.A. & Spakowitz, A.J. Subdiffusive motion of a polymer composed of subdiffusive monomers. *Phys Rev E Stat Nonlin Soft Matter Phys* **82**, 011913 (2010).
6. Doi, M., Edwards, S. F. The Theory of Polymer Dynamics. . *Oxford: Clarendon Press.* (1986).
7. Amitai, A., Toulouze, M., Dubrana, K. & Holcman, D. Analysis of Single Locus Trajectories for Extracting In Vivo Chromatin Tethering Interactions. *PLoS Computational Biology* **11**, e1004433 (2015).

Nature Structural & Molecular Biology: doi:10.1038/nsmb.3347